Electronic Supplementary Material (ESI) for Journal of Materials Chemistry A.

Supporting Information

Electrospun Cross-linked Carbon Nanofibers Film as Free-Standing and Binder-Free Anode with Superior Rate Performance and Long-Term Cyclic Stability for Sodium Ion Storage

Xu Guo[a], Xiaoting Zhang [b], Huaihe Song[a], and Jisheng Zhou[a*]

[a] State Key Laboratory of Chemical Resource Engineering, Beijing Key Laboratory of Electrochemical Process and Technology for Materials, Beijing University of Chemical Technology, Beijing 100029, P. R. China.

[b] Graphene and Energy Storage R&D Centre, Beijing Wanyuan Industry Co., Ltd., Beijing 100176, China

* Corresponding authors: Tel/Fax: +86-10-64434916, zhoujs@mail.buct.edu.cn (J Zhou)

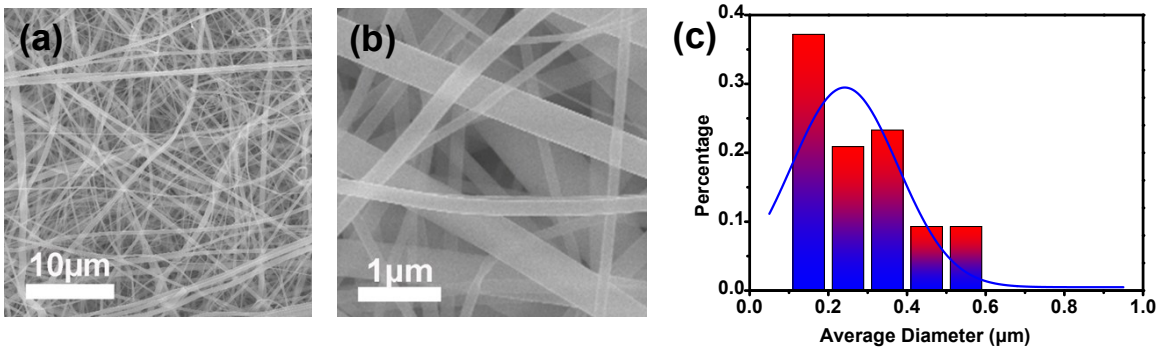

Fig. S1 (a and b) SEM images and (c) diameter distribution of PVP-NFs film.

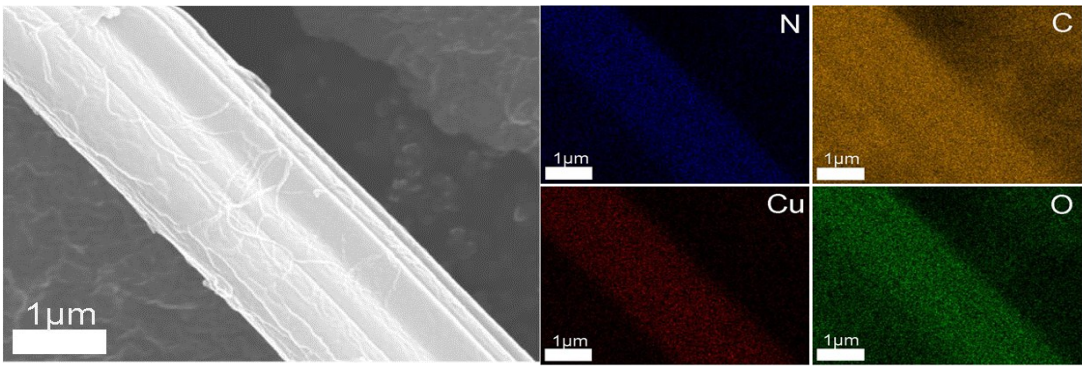

Figure. S2 Elemental mapping analysis of Cu-PVP-NFs-0.5.

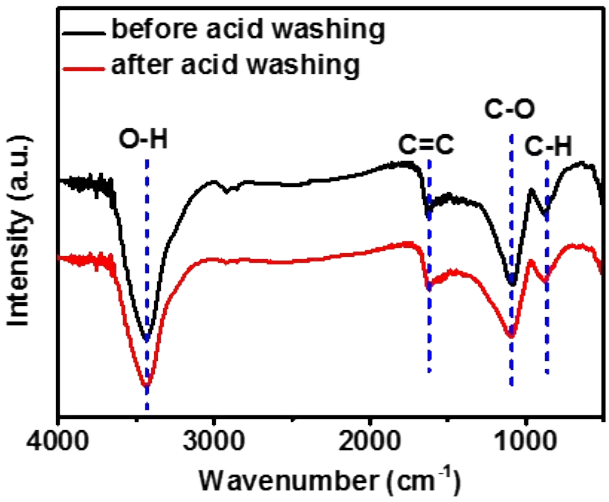

Fig. S3 FT-IR of CL-CNFs-0.5 before and after acid washing.

Table. S1 FT-IR vibrational peaks in the selected wavenumber ranges of PVP-NFs film and Cu-PVP-NFs-0.5 film.

	PVP-NFs [cm^{-1}]	Cu-PVP-NFs-0.5 [cm^{-1}]
(C=O) stretch	1650	1643
pyrrolidinyl groups	1457	1465
	1427	1427
	1380	1380
C-N stretch + CH2 wag	1288	1288

Table. S2 XPS binding energy peak positions of PVP-NFs film and Cu-PVP-NFs-0.5 film.

	PVP-NFs [eV]	Cu-PVP-NFs-0.5 [eV]
N1s	399.4	399.4
O1s	531.1	531.6

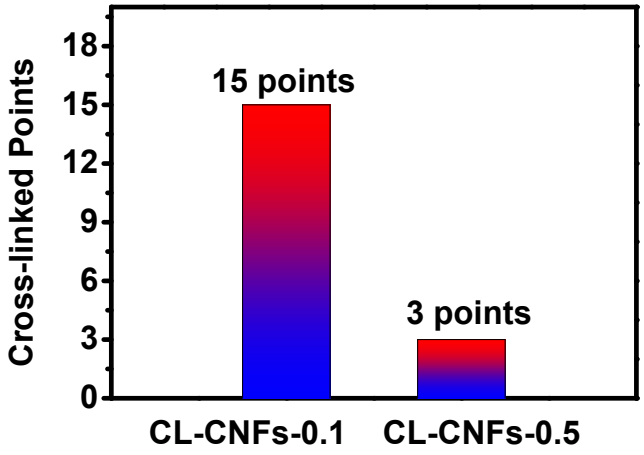

Fig. S4 Cross-linked points of single fiber of CL-CNFs-0.1 and CL-CNFs-0.5 at the length of 100 µm.

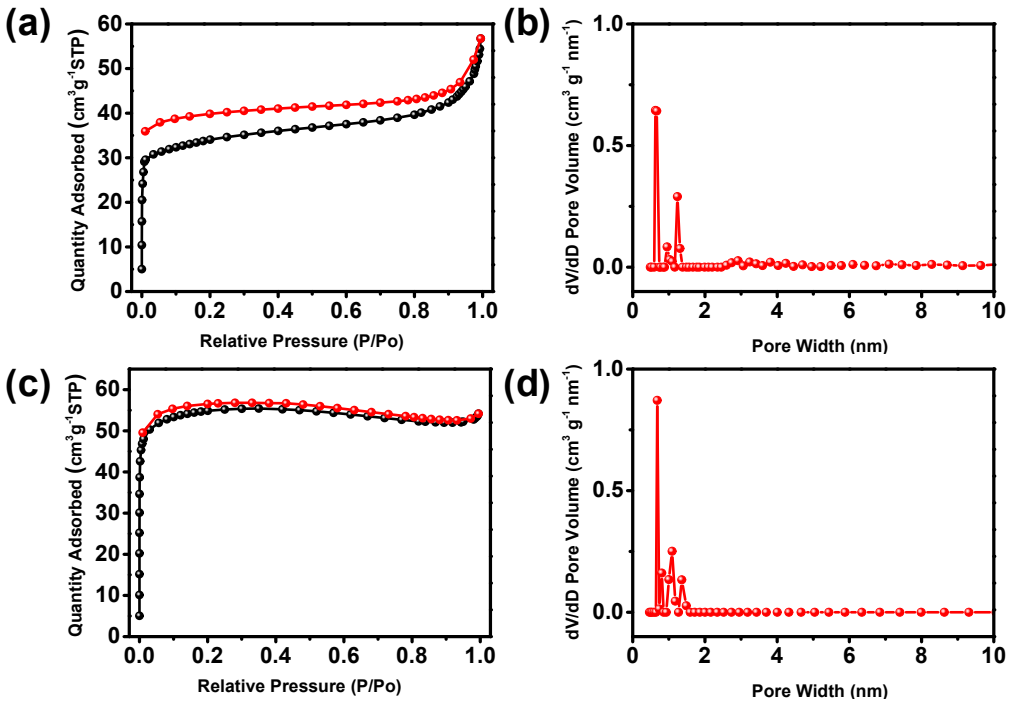

Fig. S5 N_2 adsorption/desorption isotherm curves of (a) CNFs and (c) CL-CNFs-0.5 film, pore size distributions of (b) CNF and (d) CL-CNFs-0.5 film.

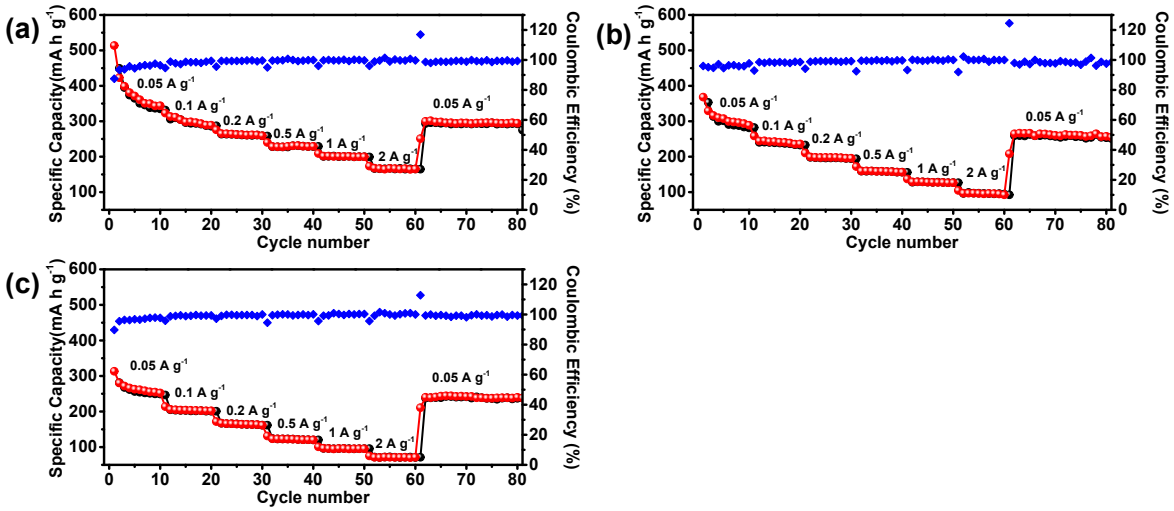

Fig. S6 Rate performances and coulombic efficiencies of (a) CL-CNFs-0.1, (b) CL-CNFs-0.5 and (c) CNFs.

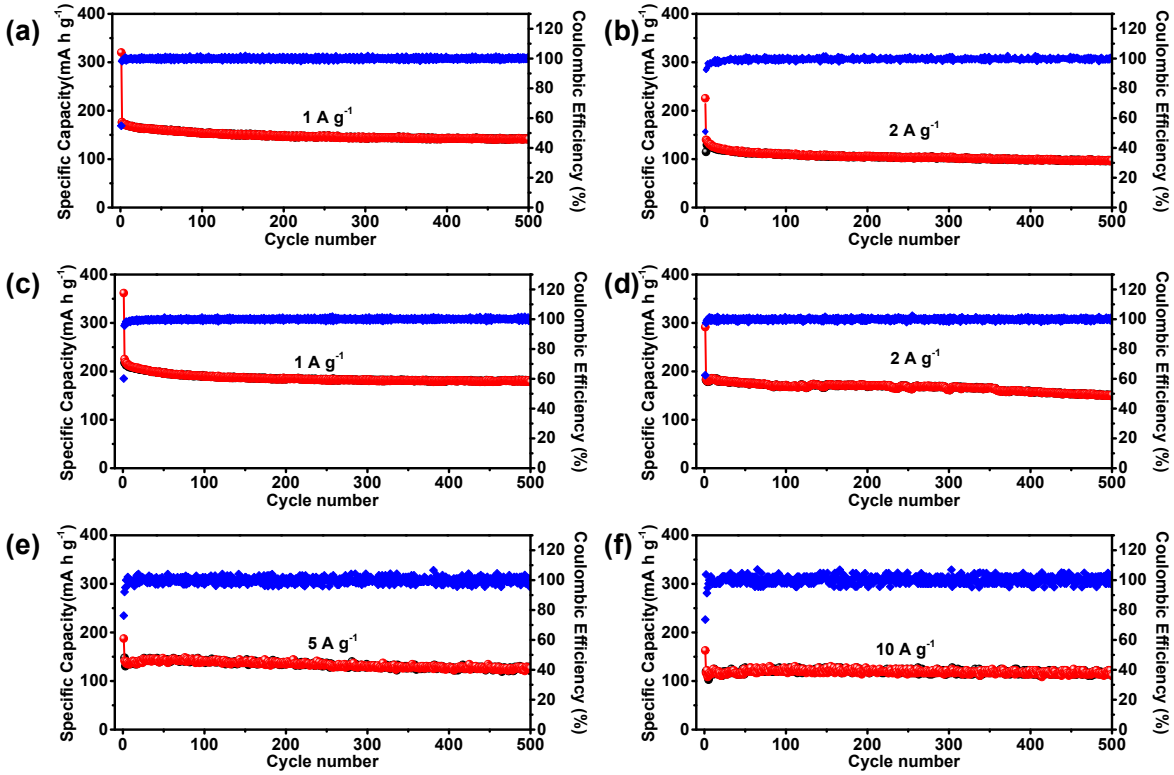

Fig. S7 Long term cycling performances and coulombic efficiencies of CL-CNFs-0.5 at (a) 1 A g^{-1} and (b) 2 A g^{-1}. Long term cycling performances and coulombic efficiencies of CL-CNFs-0.1 at (c) 1 A g^{-1}, (d) 2 A g^{-1}, (e) 5 A g^{-1} and (f) 10 A g^{-1}.

Table. S3 Comparison of our CL-CNFs-0.1 film with other carbon nanofibers that served as anode of SIBs reported by previous related works.

	Materials	Method of making anode	Reversible capacity	Rate capability	Ref
CFs	**PAN**	**Slurry coating**	**233 mA h g^{-1} at 50 mA g^{-1}**	**110 mA h g^{-1} at 2 A g^{-1}**	**S1**
P-HCNFs	**PCL/PPy**	**Slurry coating**	**319 mA h g^{-1} at 50 mA g^{-1}**	**86 mA h g^{-1} at 0.5 A g^{-1} 80 mA h g^{-1} at 1 A g^{-1} 80 mA h g^{-1} at 2 A g^{-1}**	**S2**
N-CNF	**PAN**	**Slurry coating**	**299 mA h g^{-1} at 50 mA g^{-1}**	**184 mA h g^{-1} at 0.5 A g^{-1} 159 mA h g^{-1} at 1 A g^{-1}**	**S3**
CFs	**PVC**	**Slurry coating**	**271 mA h g^{-1} at 12 mA g^{-1}**	**247 mA h g^{-1} at 0.24 A g^{-1}**	**S4**
PCFs	**PAN/Asphalt**	**Free-standing film**	**240 mA h g^{-1} at 100 mA g^{-1}**	**215 mA h g^{-1} at 0.5 A g^{-1} 195mA h g^{-1} at 1 A g^{-1} 178 mA h g^{-1} at 2 A g^{-1}**	**S5**
PAN-CNFs	**PAN**	**Free-standing film**	**261 mA h g^{-1} at 20 mA g^{-1}**	**50 mA h g^{-1} at 0.8 A g^{-1} 75 mA h g^{-1} at 1 A g^{-1}**	**S6**
CFs	**PAN/Humic Acid**	**Free-standing film**	**271 mA h g^{-1} at 20 mA g^{-1}**	**120 mA h g^{-1} at 0.8 A g^{-1} 75 mA h g^{-1} at 1 A g^{-1}**	**S7**
Lignin-based CNFs	**PAN/Refined Lignin**	**Free-standing film**	**292 mA h g^{-1} at 20 mA g^{-1}**	**100 mA h g^{-1} at 0.8 A g^{-1} 80 mA h g^{-1} at 1 A g^{-1}**	**S8**
PF-CNFs	**PAN/Refined Fulvic Acid**	**Free-standing film**	**248 mA h g^{-1} at 100 mA g^{-1}**	**120 mA h g^{-1} at 0.8 A g^{-1} 75 mA h g^{-1} at 1 A g^{-1}**	**S9**
P-CNFs	**PAN/F127**	**Free-standing film**	**280 mA h g^{-1} at 50 mA g^{-1}**	**200 mA h g^{-1} at 1 A g^{-1} 164 mA h g^{-1} at 2 A g^{-1} 90 mA h g^{-1} at 5 A g^{-1} 60 mA h g^{-1} at 10 A g^{-1} 40 mA h g^{-1} at 20 A g^{-1}**	**S10**
N-CNF	**PI**	**Free-standing film**	**564 mA h g^{-1} at 100 mA g^{-1}**	**290 mA h g^{-1} at 1 A g^{-1} 250 mA h g^{-1} at 2 A g^{-1} 200 mA h g^{-1} at 5 A g^{-1} 180 mA h g^{-1} at 10 A g^{-1} 154 mA h g^{-1} at 15 A g^{-1}**	**S11**
CL-CNFs-0.1 film	**PVP**	**Free-standing film**	**449 mA h g^{-1} at 50 mA g^{-1}**	**205 mA h g^{-1} at 1 A g^{-1} 170 mA h g^{-1} at 2 A g^{-1} 148 mA h g^{-1} at 5 A g^{-1} 121 mA h g^{-1} at 10 A g^{-1}**	**This work**

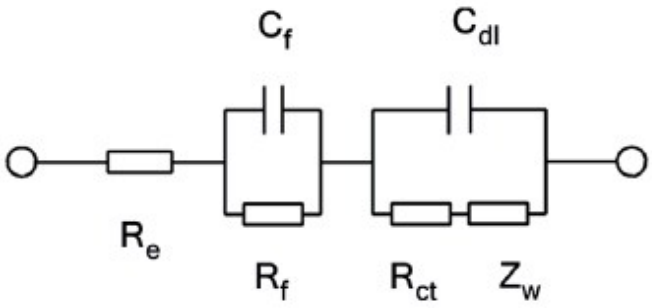

Figure. S8. Equivalent circuit: R_e is the electrolyte resistance; C_f and R_f are the capacitance and resistance of the surface film formed on the electrodes, respectively; C_{dl} and R_{ct} are the double-layer capacitance and charge-transfer resistance, respectively; Z_w is the Warburg impedance related to the diffusion of sodium ions into the bulk electrodes, and could be represented as $Zw=Y_o(j\omega)^{-0.5}$ where the Y_o is a coefficient of Warburg impedance about both the surface and the electroactive species that independs of frequency, j is imaginary part and ω is angular frequency.

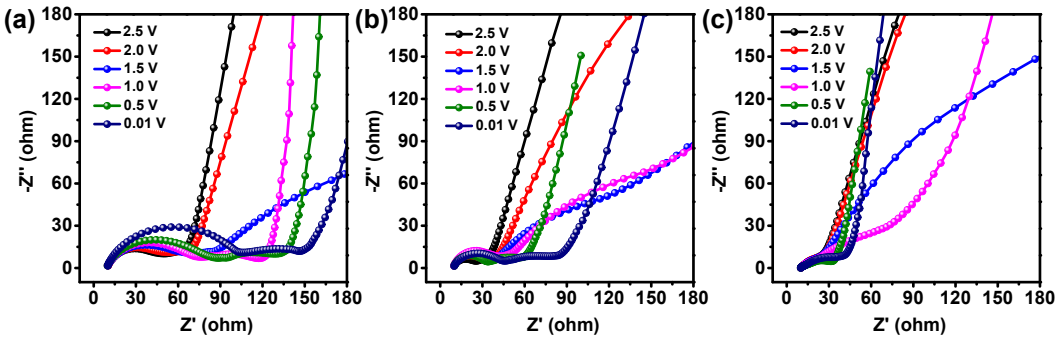

Fig. S9 EIS spectra of (a) CNFs, (b) CL-CNFs-0.5 and (c) CL-CNFs-0.1 obtained at different discharge voltage during the second discharge process at the current density of 100 mA g^{-1}.

Table. S4 Fitting results of the EIS curves in Fig. S9. using the equivalent circuit in Fig. S8.

	Open Voltage [V]	R_e [Ω]	R_f [Ω]	R_{ct} [Ω]	C_f [μF]	C_{dl} [μF]	Y_o [10^3 S $s^{-0.5}$]
CNFs	2.5	10.6	20.9	32.8	1.1	0.61	2.02
	2.0	11.0	22.9	33.3	0.40	0.65	2.12
	1.5	11.1	24.5	42.6	0.37	0.75	3.22
	1.0	13.7	48.5	33.9	0.34	145	1.41
	0.5	14.3	57.6	36.4	0.36	316	11.4
	0.01	11.8	76.7	36.4	0.32	17	20.3
CL-CNFs-0.5	2.5	9.9	11.4	18.2	0.88	2.2	4.22
	2.0	9.9	14.9	19.7	0.86	1.8	4.75
	1.5	9.9	15.4	21.3	0.86	1.9	8.68
	1.0	10.1	20.2	27.5	0.70	1.4	5.48
	0.5	10.7	20.8	19.9	1.1	546	29.7
	0.01	11.7	28.9	27.2	0.83	443	28.6
CL-CNFs-0.1	2.5	10.5	4.2	14.9	6.4	2.2	3.10
	2.0	10.3	3.6	14.7	5.2	1.8	5.14
	1.5	10.3	3.7	14.1	6.2	1.9	4.46
	1.0	10.2	3.1	27.6	5.4	1.4	11.5
	0.5	10.2	2.9	14.5	7.0	443	25.8
	0.01	10.3	2.8	21.5	7.2	546	65.8

Reference

S1 T. Chen, Y. Liu, L. Pan, T. Lu, Y. Yao, Z. Sun, D.H.C. Chua, Q. Chen, J. Mater. Chem. A, 2 (2014) 4117-4121.

S2 L. Zeng, W. Li, J. Cheng, J. Wang, X. Liu, Y. Yu, RSC Adv., 4 (2014) 16920-16927.

S3 J. Zhu, C. Chen, Y. Lu, Y. Ge, H. Jiang, K. Fu, X. Zhang, Carbon, 94 (2015) 189-195.

S4 Y. Bai, Z. Wang, C. Wu, R. Xu, F. Wu, Y. Liu, H. Li, Y. Li, J. Lu, K. Amine, ACS Appl. Mater. Interfaces, 7 (2015) 5598-5604.

S5 Y. Qi, W. Fan, G. Nan, Mater. Lett., 189 (2017) 206-209.

S6 J. Jin, Z.Q. Shi, C.Y. Wang, Electrochim. Acta, 141 (2014) 302-310.

S7 P.Y. Zhao, B.J. Yu, S. Sun, Y. Guo, Z.Z. Chang, Q. Li, C.Y. Wang, Electrochim. Acta, 232 (2017) 348-356.

S8 J. Jin, B.J. Yu, Z.Q. Shi, C.Y. Wang, C.B. Chong, J. Power Sources, 272 (2014) 800-807.

S9 P.Y. Zhao, J. Zhang, Q. Li, C.Y. Wang, J. Power Sources, 334 (2016) 170-178.

S10 W. Li, L. Zeng, Z. Yang, L. Gu, J. Wang, X. Liu, J. Cheng, Y. Yu, Nanoscale, 6 (2014) 693-698.

S11 S. Wang, L. Xia, L. Yu, L. Zhang, H. Wang, X.W.D. Lou, Adv. Energy Mater., 6 (2016) 1502217-1502224.